A&A 428, 459–467 (2004)
DOI: 10.1051/0004-6361:20041619

Astronomy & Astrophysics

Intermediate-age globular clusters in early-type galaxies: Better age determinations by adding *U*-band observations to the *V*, *I*, *K* datasets⋆,⋆⋆

M. Hempel and M. Kissler-Patig

European Southern Observatory, Karl-Schwarzschild-Str. 2, 85748 Garching, Germany
e-mail: [mhempel;mkissler]@eso.org

Received 8 July 2004 / Accepted 19 August 2004

Abstract. This paper represents an extension to a series of publications on combined optical and near-infrared photometry of globular cluster systems in early-type galaxies. Based on color-color diagrams the cumulative age distributions of their globular cluster systems have been derived and revealed intermediate age clusters in two galaxies, namely NGC 4365 and NGC 5846. The extension of this observations towards the blue wavelength range was performed in order to increase the age resolution of photometric studies. In this paper we present the results of U-band observations of NGC 4365 and NGC 5846 and their combination with previously obtained V, I and K_s-band photometry. $(U - I)$ vs. $(V - K_s)$ color–color diagrams are used to derive the cumulative age distribution. The later is compared to simulated globular cluster systems of known age and size composition in order to set constrains on relative ages and size of the sub-populations.

Key words. galaxies: star clusters – galaxies: elliptical and lenticular, cD

1. Introduction

Photometric studies on globular cluster systems are of growing interest for our understanding of how and when galaxies form and how they evolve. Being less expensive in observing time than spectroscopy, they are the first step in surveys on the age structure of globular cluster systems. Due to the age-metallicity degeneracy (e.g. Worthey 1994) photometry alone can, in terms of accuracy in the age determination, not compete with spectroscopic data. Nevertheless, single stellar population (SSP) models (e.g. by Maraston 2000; Bruzual & Charlot 1993, 2003; Vazdekis 1999) allow the detection based on color distributions of globular cluster sub-populations differing in age by several Gyr. With the introduction of near-infrared photometry (Kissler-Patig et al. 2002; Puzia et al. 2002; Hempel et al. 2003; Hempel & Kissler-Patig 2004, hereafter cited as Papers I, II, III and IV) the age resolution improved significantly and relative ages of globular cluster sub-populations in a galaxy could be derived.

An advantage of photometry for these type of work is that it surpasses spectroscopic investigations with regard to the observing time required to obtain data for a statistical relevant sample. As we demonstrated in Paper IV, the sample size is a key issue in our method to derive the relative age and size of globular cluster sub-populations. The latter is, as first considered by Ashman & Zepf (1992), linked to the formation scenario of a given galaxy. The accuracy to which the age and metallicity as well as extinction and mass can be determined depends strongly on wavelength coverage of the observations, as shown in a recent work by Anders et al. (2003). With the partly lifted age-metallicity degeneracy in combined optical/near-infrared photometry, the age resolution within an intermediate age population can be further improved by the coverage of the short wavelength range, sensitive to age of integrated stellar populations.

Thus, a more accurate age dating by including U- and/or B-band observations become possible. Also, because a hidden disadvantage of the infrared observations was the limiting magnitude and associated higher photometric errors that needs to be conceded. The latter translates directly into a finite age accuracy which prevents us from taking full advantage of the $(V - I)$ vs. $(V - K_s)$ color–color diagram. As shown in Fig. 1, $(U - I)$ improves the age resolution by a factor of ∼3 with respect to $(V - I)$ when matched with $(V - K)$ colors. As an example we compare the color difference between a 15 Gyr and a 5 Gyr old cluster population. Hereby we stay in the red color range ($(V-K_s) \geq 2.6$), where we expect to find a second generation of metal-rich globular clusters (Paper III). The $(U-I)$ color between both age populations differ by ≳0.4 mag. This is well

⋆ Based on observations at the Very Large Telescope of the European Southern Observatory, Chile (Program 71.B-0596).

⋆⋆ Based on observations made with the NASA/ESA Hubble Space Telescope, obtained from the data archive at the Space Telescope Science Institute. STScI is operated by the association of Universities for Research in Astronomy, Inc. under the NASA contract NAS 5-26555.

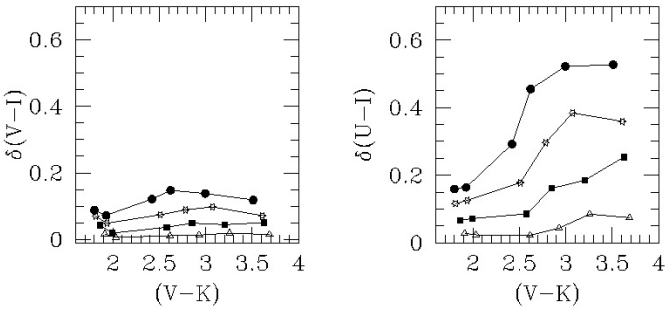

Fig. 1. Both panels show the difference in the secondary color ($(V-I)$, left or $(U-I)$, right) for a 5 (solid circles), 7 (open stars), 10 (solid squares) and 13 Gyr (open triangles) isochrone compared to a 15 Gyr old population (following the Bruzual & Charlot 2000 SSP model). The metallicity increases with $(V-K_s)$ from 0.005 $Z_\odot$ up to 2.5 $Z_\odot$.

above the error limit of 0.15 mag for both colors which we typically apply to select reliable photometry for globular clusters.

In the following, we present the results of our U-band observations of two galaxies, NGC 4365 and NGC 5846, combined with previously obtained V, I, and K_s-band data. In both galaxies intermediate age globular clusters have been found. In line with the work presented in Papers III and IV the $(U-I)$ vs. $(V-K_s)$ color–color distribution will be used to derive the cumulative age distribution and to set stronger constraints on relative age and size of the second generation of globular clusters. To show the effect of the extended wavelength range on the age distribution we will compare the results for both color combinations (i.e. $UVIK_s$ vs. VIK_s).

2. VLT/FORS1 *U*-band photometry

2.1. Observations

We have complemented our V, I and K_s-band observations of two galaxies, NGC 4365 and NGC 5846 with U-band data. The U-band exposures for both galaxies have been taken in visitor mode (ESO program 71.B–0596) with the FOcal Reducer/low dispersion Spectrograph 1 (FORS1) in imaging mode, attached to the Unit Telescope 1 (Antu) of the European Southern Observatory's Very Large Telescope (VLT). The field-of-view of FORS1's Tektronix CCD is $6\farcm8 \times 6\farcm8$, with a pixel scale of $0\farcs2$/pixel.

The data were obtained during the nights of May 6th, 7th, and 8th, and June 23th and 24th 2003. The total exposure times are 43 800 s for NGC 5846 and 38 400 s for NGC 4365. Our goal was to obtain a $S/N = 15$ for objects with $U = 25$ mag, expecting a $(U-K)$ color range ($\leq$3.5 mag) for an old (15 Gyr) stellar population at a limiting $K_s = 21.5$ mag. The total exposures were split into 1800 s observations to avoid saturation of the galaxy. Exposures, taken under photometric conditions, were used to calibrate the total exposure. The photometric zero point ZP = 25.199 ± 0.021 mag (derived using 8 standard stars) was provided by the FORS 1 quality control group.

Table 1. General information about the host galaxies NGC 5846 and NGC 4365. The references are (1): de Vaucouleurs et al. (1991); (2): Schlegel et al. (1998); (3): Buta & Williams (1995); (4): Frogel et al. (1978); (5): Tonry et al. (2001).

Property	NGC 5846	NGC 4365	Reference
RA(J2000)	15h06m29s	12h24m28s	(1)
Dec(J2000)	+01°36′25″	+07°19′03″	(1)
$B_{T,0}$	10.87	10.49	(1)
E_{B-V}	0.055	0.021	(2)
$(B-V)_o$	0.96	0.95	(1)
$(V-I)_{eff,o}$	1.28 ± 0.01	1.25 ± 0.01	(3)
$(V-K)_{eff,o}$	3.51 ± 0.01	3.29 ± 0.1	(4)
$(m-M)_V$	31.98 ± 0.20	31.55 ± 0.17	(5)
M_V	−22.07	−22.01	(1), (5)

2.2. Photometry

For both galaxies the V, I and K_s-band data have been obtained in previous observing runs and the reductions was described in detail in Papers II and III. Therefore we will restrict ourselves on detailing the U-band photometry. Measuring the instrumental magnitudes with an aperture radius of $10\farcs0$ (as used for the standard star photometry), the calibration of the short time exposure (photometric) follows the equations given below.

$$U_{\rm galaxy} = u_{\rm inst} + 25.199(\pm0.021) - 0.505\chi$$

where $U_{\rm galaxy}$ is the calibrated magnitude, $u_{\rm inst}$ is the instrumental magnitude, and χ the airmass (1.13 for NGC 5846 and 1.52 for NGC 4365). The error of the zero points (second term in the equation) includes photometric errors of each single standard star measurement and the errors of the aperture correction analysis.

The final images for both targets were obtained by averaging the 25 (NGC 5846) and 22 (NGC 4365) single exposures. Their alignment and stacking was done using the IRAF tasks *imalign* and *imcombine*. Before combining the images have been processed individually. The images were divided by a normalised masterskyflat, created from the twilight flat field exposures for each night. The photometry was carried out using SExtractor v2.1.6 (Bertin & Arnouts 1996). To calibrate the total exposure we used a single exposure taken under photometric conditions and calculated the difference in instrumental magnitude of 33 (NGC 5846) and 19 (NGC 4365) objects to the one obtained in the total exposure. This photometric offset was calculated to be 23.98(±0.021) mag in NGC 5946 and 24.01 (±0.055) mag in NGC 4365 and added to the instrumental magnitude of all detected sources. To avoid crowding effects the instrumental magnitudes were determined for a $1\farcs0$ aperture (radius) and corrected for the $10\farcs0$ radius used for the zero point determination.

Finally, all magnitudes were corrected for Galactic foreground reddening using the reddening values of Table 1 and the extinction curves of Schlegel et al. (1998). The corrections for NGC 5846 and NGC 4365 are $A_U = 0.299$ mag and $A_U = 0.115$ mag.

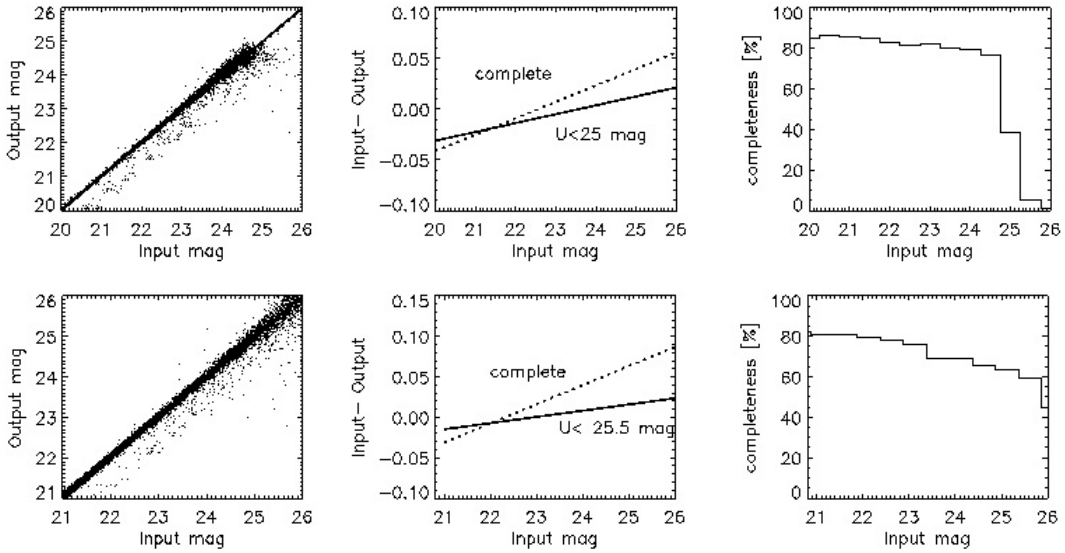

Fig. 2. *Left*: comparison between input and measured U-band magnitude of artificial objects (1000 objects per 0.5 mag). The dotted line represents the best fit to the complete data set whereas the solid line includes only objects with $U < 25$ mag (*top*: NGC 4365) and $U < 25.5$ mag (*bottom*: NGC 5846). *Central*: difference between an ideal detection (input = output magnitude) and the best fit. *Right*: detection rate for NGC 4365 and NGC 5846. Objects brighter than 25 mag (NGC 4365), respectively 25.5 mag (NGC 5846) are detected to at least 70%.

We detected 514 objects in NGC 4365 and 1201 objects in NGC 5846 on the final U-band images using SExtractor (Bertin & Arnouts 1996). For later analysis we selected only objects for which a photometric error of $\Delta U \leq 0.1$ mag had been determined. For both targets this limit is only exceeded close to the detection limit of our observations. The remaining samples contained 498 and 1198 objects in NGC 4365 and NGC 5846, respectively.

3. Combined *U, V, I, K* photometry

Given the depth of the V-and I-band exposures (obtained with WFPC2 on board the Hubble Space Telescope) the detection limit in the combined photometry will be driven by the U- and K_s-band observations. From previous work we recall the detection limits for the K_s-band to be 21.5 mag for NGC 5856 and 20.25 mag for NGC 4365. Typical $(U - K)$ colors as derived from the SSP model isochrones (e.g. Bruzual & Charlot 1993) for stellar populations with ages between 1 and 15 Gyr range between $(1 \leq U - K_s \leq 4)$. Thus, U-band data as deep as $U = 25.5$ mag and $U = 24.25$ mag would be required for NGC 4365 and NGC 5846 respectively, in order not to introduce a additional limitation due to the U-band.

Using the *addstar* task within IRAF we test the reliability of the Sextractor detection within this magnitude range. As shown in Fig. 2 (left panel) the U-band magnitude for artificial objects is recovered by Sextractor up to $U_{\rm lim} = 25$ mag and 25.5 mag for NGC 4365 and NGC 5846. In both cases the best fit deviates from an "input magnitude = output magnitude" relation by an amount smaller than the photometric error. The difference between such an ideal detection and real measurements is shown in the central panels of Fig. 2. The dotted line represents the best fit to the magnitude difference for all input particles, whereas for objects with $U \leq U_{\rm lim}$ the best fit follows the solid line. Objects brighter than 25.0 and 25.5 mag (correct detection) are detected with a 70% probability as seen in the right panels of Fig. 2. If we apply additionally the above mentioned error cut for the U-band detections (0.1 mag) we find that objects fainter than $U = 24.2$ mag and $U = 25.0$ mag will not be detected in NGC 4365 and NGC 5846, respectively.

3.1. NGC 4365

The color–magnitude diagram (CMD) and the color–color diagrams of NGC 4365 are given in Figs. 3 and 4. The histogram on top of the CMD shows the complete sample as an open histogram whereas the hatched regions mark the selected sample ($\delta(U - K) \leq 0.15$ mag). As in the $(V - K_s)$ color distribution (Paper II) we find two distinct populations in the $(U - K_s)$ color distribution, although the sample is too small to allow a well defined double Gaussian fit to the data, in order to determine the mean color of both sub-populations. We compare the color–color diagrams using V, I and K_s band observations (top panel) or U, V, I and K_s-band data (bottom panel) in Fig. 4, which demonstrates the age resolution as a function of different color combinations. The remaining cluster in the sample are more widely spread in the color space and their ages can be defined more reliably by model isochrones if U-band observations are included.

3.2. NGC 5846

Taken from Paper III (see Fig. 3 therein), and later confirmed by spectroscopy, NGC 5846 contains as well as NGC 4365, a significant fraction of *intermediate age* globular clusters, for which we now aim at a more precise age estimate. Shown in Figs. 5 and 6 are the color–magnitude diagram for NGC 5846 and the color–color distribution. As in NGC 4365 the number of very red (in $U - K$) objects is cut down, but the bimodal

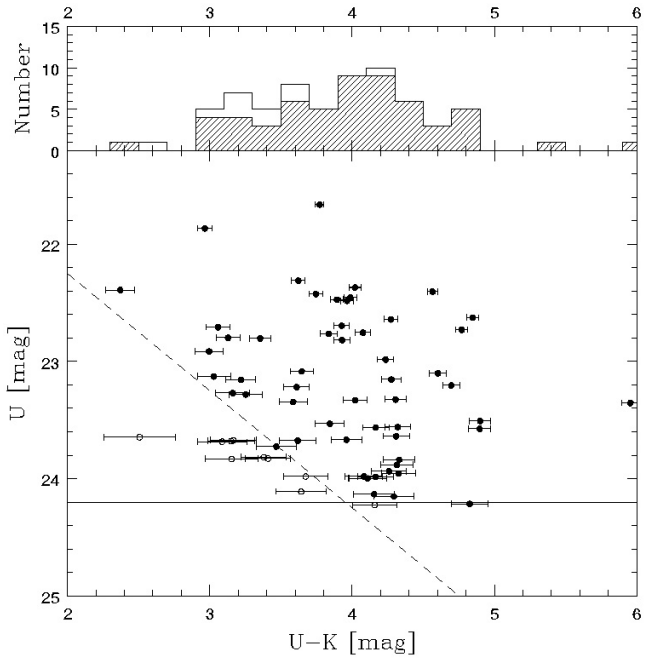

Fig. 3. U vs. $(U-K)$ color–magnitude diagram for NGC 4365. The top panel shows the color distribution of all (open histogram) and selected (shaded histogram). As selection criterion we applied a error cut for $(U-K)$ with $\delta(U-K) \leq 0.15$ mag. The lower sub-panel shows the CMD. Here the filled circles mark the selected clusters while open circles indicate rejected objects. The dashed line marks the limiting magnitude in the K_s-band ($K = 20.25$ mag) and the solid line the U-band limit for $\Delta U \leq 0.1$ mag.

color distribution can still be seen in Fig. 5 although a fit to the color distribution suffers from the low number statistics. Nevertheless, at this stage we are interested in the age resolution and will settle with the fact that our derived size ratios between the globular cluster sub-populations refer to a strongly biased fraction of the total globular cluster system (see below).

3.3. Color–color diagrams for NGC 4365 and NGC 5846

In Papers II and III of this series color–color diagrams of combined optical and near-infrared photometry were used to detect globular cluster sub-populations with different ages. In both galaxies up to 80% of the objects included in the calculation were assigned to an intermediate age population, although see Papers III and IV for caveats on this estimates. Using the higher resolution power of $(U-I)$ vs. $(V-K)$ color–color diagrams compared to $(V-I)$ vs. $(V-K)$ (see Fig. 1) we aim at a more accurate age determination for the second generation of globular clusters. This is achieved as shown in Figs. 4 and 6 (lower panels), where we find the globular cluster colors much closer linked to a specific isochrone, resulting in only a small age uncertainty for a given SSP model.

After matching the U, V, I, and K_s band observations and applying the error selection criterion the globular cluster sample contains 62 objects in NGC 4365 and 51 objects in NGC 5846. In the discussion of the results, the relative size and

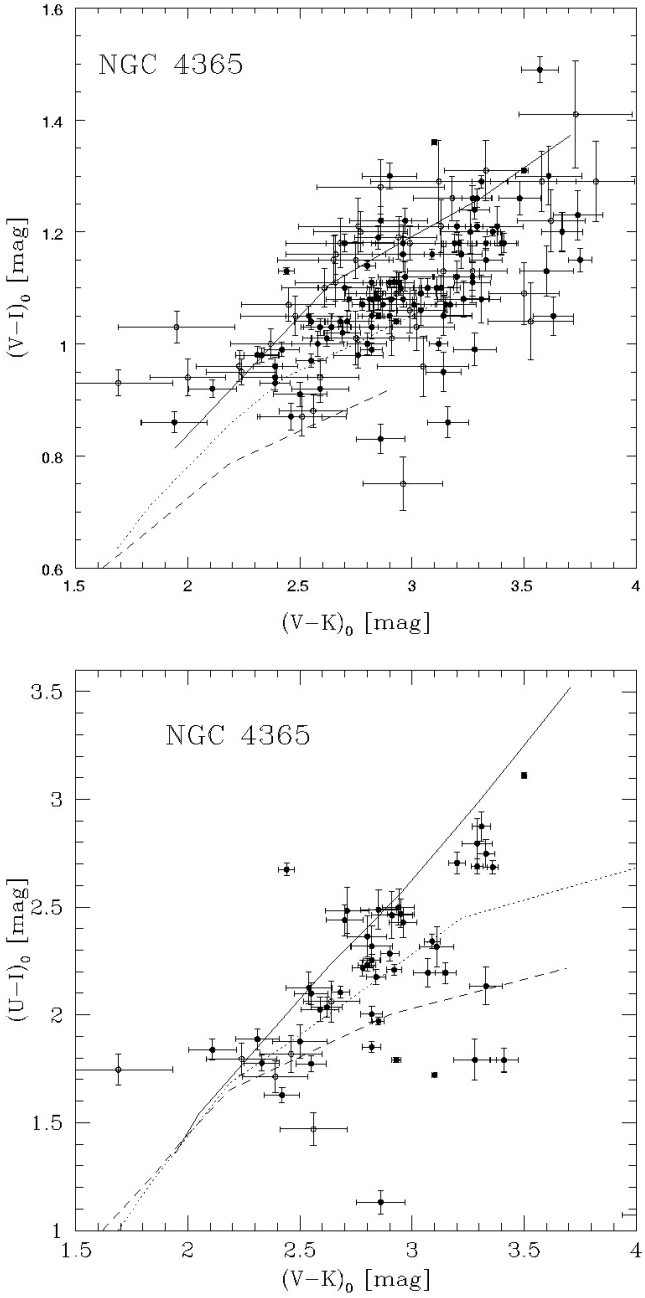

Fig. 4. $(V-I)$ vs. $(V-K)$ and $(U-I)$ vs. $(V-K)$ color–color diagram for NGC 4365. All data are corrected for galactic foreground reddening (Table 1). As example the 1 (dashed), 5 (dotted), and 15 (solid) Gyr isochrones (Bruzual & Charlot 1993) are marked.

age of cluster sub-populations, we have to weight the effects of an improved age resolution against the diminished globular cluster samples. The limiting bands are U and K_s. The first will favor detections at low $(V-I)$, the second at high $(V-K_s)$. Thus, our detection probability decreases in the color-color diagram from the bottom right to top left. In other word, young and metal-rich globular clusters are now favored and both samples biased towards these.

The $(U-I)$ and $(V-K_s)$ color ranges in which globular cluster are found is defined by the age and metallicity range. Following the SSP model isochrones (Bruzual & Charlot 2000), globular clusters with an age of 1 Gyr and a metallicity

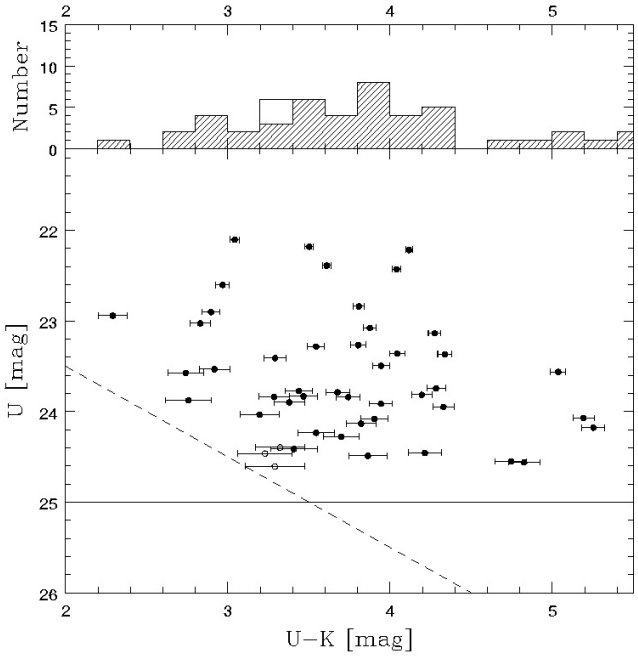

Fig. 5. U vs. $(U-K)$ color–magnitude diagram for NGC 5846 (dereddened, Schlegel et al. 1998). The limiting K_s-band magnitude is K_s = 21.5 mag, panels and symbols are indicated as in Fig. 3). The horizontal line at U = 25.0 mag marks the U-band limit for detections with $\Delta U \leq 0.1$ mag.

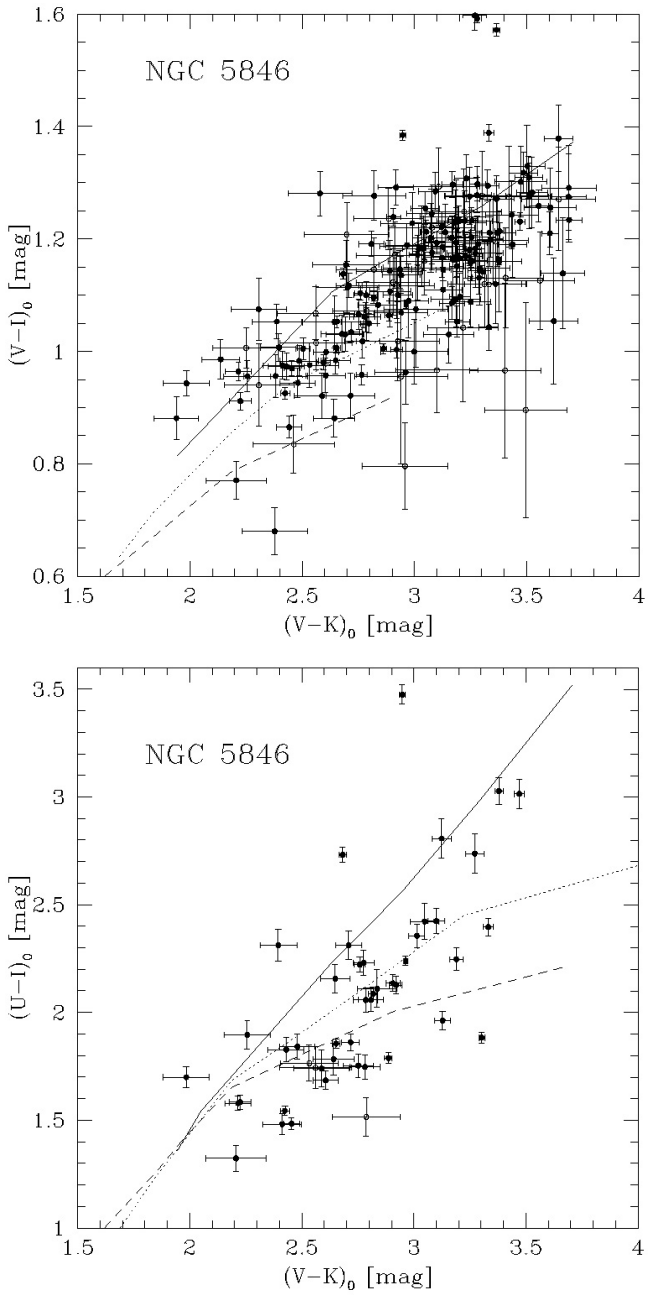

Fig. 6. Color–color diagrams (*top* $(V-I)$ vs. $(V-K)$, *bottom*: $(U-I)$ vs. $(V-K)$) for NGC 5846. Solid and open symbols mark data with photometric errors below, respectively above 0.15 mag. The model isochrones (Bruzual & Charlot 2000) for a 15 Gyr (solid), a 2 Gyr (dotted) and a 1 Gyr (dashed) SSP are shown.

of up to $2.5 \times Z_\odot$ will show a $(V-K_s) \leq 2.9$. The upper limit $(V-K_s) \leq 3.6$, which we apply for the determination of the age distributions, refers to a 15 Gyr isochrone. The latter sets also an upper limit to $(U-I)$ of 3.6 mag.

A major issue in our analysis are various bias effects. Any quantitative statement about the size of globular cluster sub-populations requires careful considerations of selection effects, either related to the spatial distribution or to the completeness in the observations. As shown in Fig. 7 the observations were carried out with the fields of view centered on the galaxy. So far data in all 4 filter bands are only available for objects within $\leq$1.5 $R_{\rm eff}$ of both galaxies, i.e. their innermost regions. Simulations of merger processes (e.g. Hibbars & Mihos 1995) and observations of recent merger remnants (e.g. NGC 7252, Schweizer & Seitzer 1998) have shown that the gas, from which globular clusters will form during a galaxy-galaxy merger, funnels towards the center of the merger, within a few 100 Myr. A much higher fraction of intermediate age globular clusters is expected in the center than in the outskirts of the globular cluster system. Therefore we expect our sample to contain a high fraction of intermediate/young age globular clusters. We have also to consider that only globular clusters with a high bolometric magnitude will be detectable in all four filter bands and this selection will create an additional bias in favor of the most massive and youngest objects as it can be seen in Fig. 8. There we compare the U-band luminosity function for NGC 4365 and NGC 5846 within the ISAAC field of view. The open histogram includes all U-band detections, whereas the shaded histogram refers only to objects which could also be detected in the near-infrared. Finally, as mentioned above the combination of the limiting magnitudes in both U and K-band biased the sample in favor of the young and metal-rich globular clusters, discriminating against the old metal-poor, as well as against the old, metal-rich globular clusters.

As a conclusion, we can state that the addition of the U-band greatly improves the age resolution, and thus allows to better quantify the ages of sub-populations. It does so, however, at the cost of introducing strong biases with respect to the numbers of clusters detected in each age/metallicity sub-population,

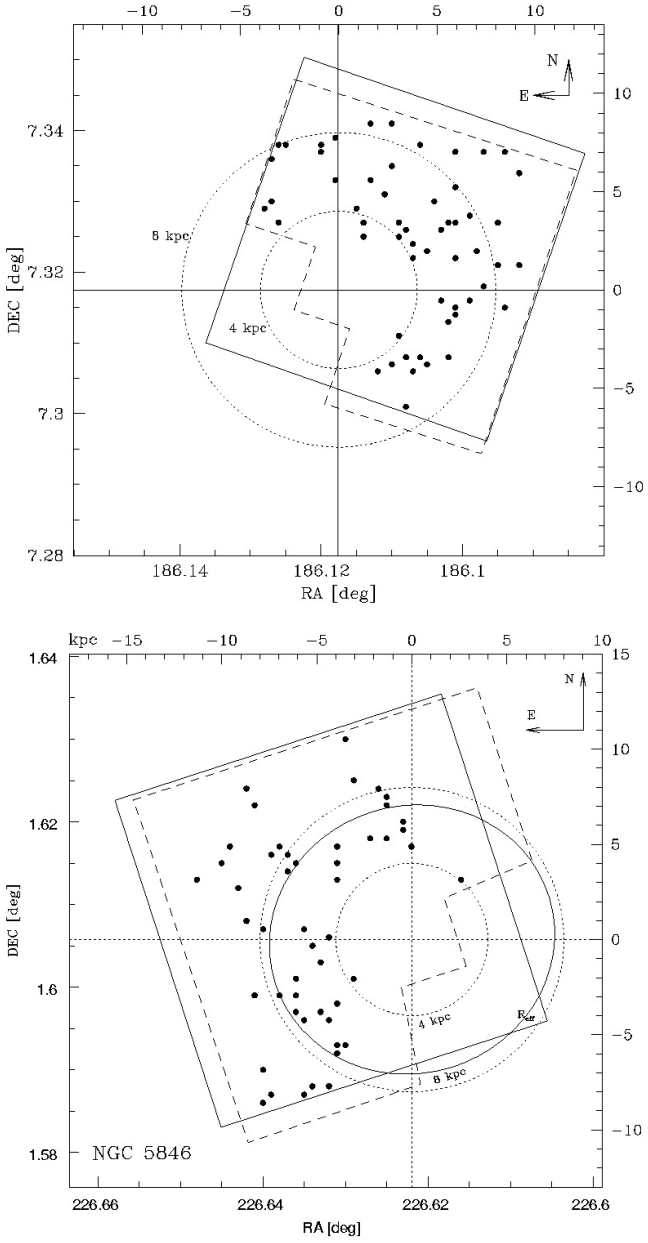

Fig. 7. Field of view for the NGG 4365 (*top panel*) and NGC 5846 (*bottom panel*) data on the sky. The data (solid circles) show all objects for which data in all 4 bands, U, V, I, and K_s are available. Due to the small field of view covered by ISAAC our complete data set is limited by the K_s-band observations (solid line) and the larger HST/WFPC2 images (dashed line) and we abandon from superimposing the much larger FORS1 field of the U-band observations.

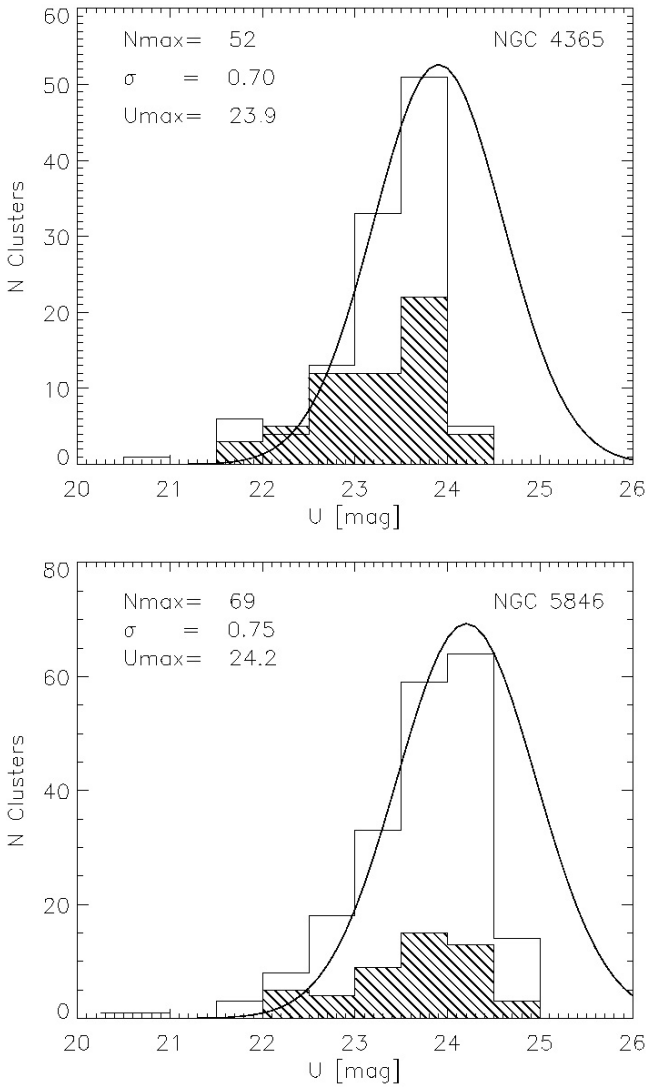

Fig. 8. Luminosity distributions for NGC 4365 (*top*) and NGC 5846 (*bottom*). The open histograms represent the total sample of objects found within an □ 2.′5 field of view (VLT/ISAAC). The shaded histogram contains objects for which counterparts in V, I and K_s could be found. An error cut was set to $\delta U \leq 0.1$ mag.

so that the current U, V, I, K dataset is not appropriate to derive relative sizes of the different sub-populations.

4. Age sub-populations

4.1. Cumulative age distribution

Following the procedure described in Papers III and IV the cumulative age distributions were derived for NGC 4365 and NGC 5846, and are shown in Fig. 9. The contamination with background objects is considered to be not significant, based on the selected color range and the corresponding HDF-South data.

The cumulative age distribution gives a first indication for age sub-populations but the comparison with simulated cluster systems (Paper IV) allows to set constraints on their relative age and size. In our previous simulations (Papers III and IV) we assumed the first generation of globular clusters to be 15 Gyr old (see Fig. 17 in Paper IV). In agreement with the latest WMAP results (e.g. Bennet et al. 2003; Spergel et al. 2003) we are now working with an age of 13 Gyr for the old cluster population. Thus we expect a small change in the ratio between the sub-populations and the age of the intermediate age population.

The age difference between both populations stays more or less constant at ∼10 Gyr. On the other side the results are in different way affected by the extended color range as we will discuss in Sect. 4.2 (see also Sect. 3).

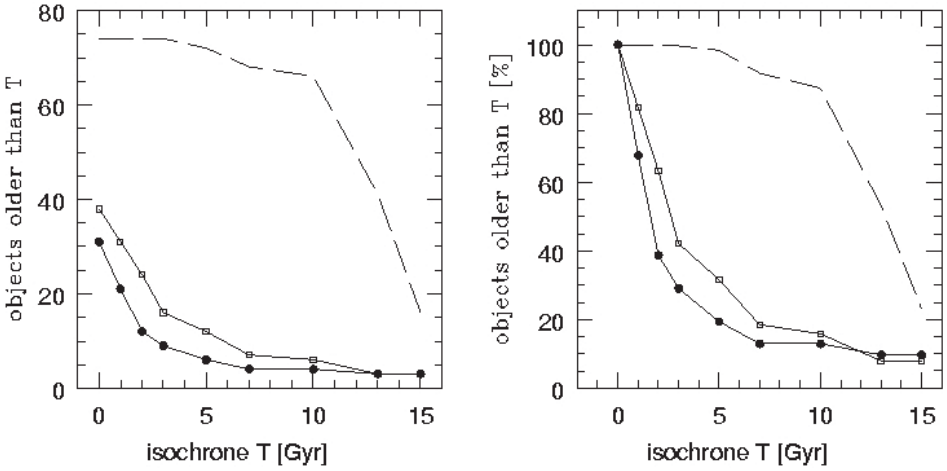

Fig. 9. Cumulative age distribution in the globular cluster systems of NGC 4365 and NGC 5846. For the age dating we applied the SSP model by Bruzual & Charlot (2000). The left panel shows the number of objects being older than a specific isochrone and the right panel the relative distribution (normalised to the total number of objects). Open symbols represent NGC 4365 globular clusters and closed symbols NGC 5846 objects, respectively. As an example the age distribution for a simulated cluster systems (13 Gyr old objects only) is marked by the dashed line.

4.2. Impact of the sample size

In Fig. 10 we present the results for the comparison between the cumulative age distribution of simulated globular cluster samples with varying sample size. By combining the previous V, I and K_s band data with U-band observations, we increase the age resolution on one side, but the number of clusters drops significantly. In the simulations we work with 120 objects within the red color range, where we expect the majority of the second generation clusters. Due to the different size of observed and simulated globular cluster systems we need to test the stability of our χ^2 test, as we did in Paper IV for V, I and K_s-band photometry. To do so we compare the cumulative age distribution of simulated globular cluster systems (hereafter called *original*) consisting of 10, 20, 60, 120, and 240 red globular clusters, with the complete model set. For our *originals* we assume a 50%- mix of 13 Gyr and 3 Gyr old objects. The χ^2-test between *original* and model set should return the correct age and size combination of the former. The models are built as combinations of a 13 Gyr old first generation and a second population with an age of 1, 1.5, 2, 3, 5, 7, or 10 Gyr. As described in Papers III and IV the size ratio changed between a 100% old population and a pure young/intermediate population in 10% increments. We note that for each parameter set we derive the age distribution as the statistical mean of 1000 separate simulations per age and size composition.

In Paper IV the stability test for the comparison between age distributions of samples of different sizes and our model database based on $(V - I)$ vs. $(V - K_s)$ color–color diagrams shows that $\gtrsim$100 object are needed in this approach. Using $(U - I)$ vs. $(V - K_s)$ color–color diagrams leads to stable result for a smaller sample as an increased age resolution compensates for the reduced sample size. As we can see in Fig. 10 for samples of $\geq$60 objects in total age and size are recovered. The model which fits best to the "original" data set is found to consist of two equal size sub-populations with ages of 3 Gyr and 13 Gyr, i.e. the input model parameters. A sample size of 62 and 51 in NGC 4365 and NGC 5846 is therefore sufficient to allow a χ^2-test which will not be affected significantly by number statistics.

4.3. Age structures in NGC 4365 and NGC 5846

Given the high age resolution of the $(U - I) - (V - K)$ combination, a few conclusions about the age structure in NGC 4365 and NGC 5846 can already been drawn from the color-color diagrams for both targets.

In NGC 4365 (Fig. 4, bottom panel) the majority of the globular clusters has a $(V - I)$ color which corresponds to an age $\gtrsim$2 Gyr, whereas only a few objects are found to be even bluer than the 1 Gyr model isochrone.

In NGC 5846 the situation is different. In Fig. 6 (bottom panel) we find the majority of objects to be younger than 2 Gyr and only a very small fraction of old objects (i.e. $\geq$5 Gyr).

The results of the χ^2-tests for the comparison between the cumulative age distribution of observed and simulated globular cluster systems are shown in Fig. 11. Results from U, V, I, K datasets and the V, I, K datasets alone are compared (top vs. bottom panel). We confirm the existence of an intermediate age population of globular clusters in both galaxies, being $\sim$10 Gyr younger than the first generation of clusters (assumed age: 13 Gyr). This age difference agrees well with the results assuming a first generation age of 15 Gyr in the models used in Paper IV and finding the best fitting model to contain a second population at age 3–5 Gyr. As expected for the extended wavelength range the relative age and size of the globular cluster populations are now much better defined, as shown by the χ^2- contours (Fig. 11, lower panel). Nevertheless- working with globular clusters detected in U, V, I and K_s introduces selection effects (see Sect. 3): the method favors the young population. In case of NGC 4365 the cumulative age distribution is best fitted by a model containing $\sim$40% of 13 Gyr old objects and $\sim$60% clusters which are 2 Gyr old. In NGC 5846 the age of the

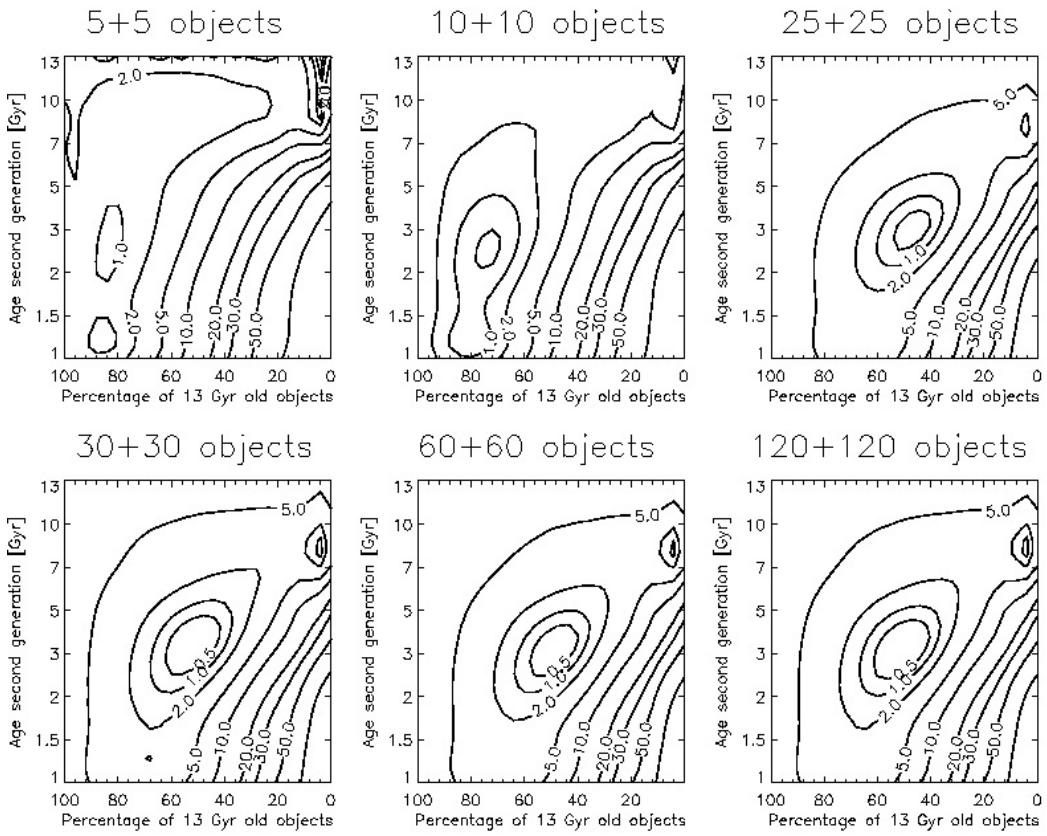

Fig. 10. Result of the χ^2-test comparing the cumulative age distribution of simulated systems consisting of 10, 20, 60, 120 and 240 red objects, respectively. The red populations is split into 50% old (13 Gyr) and 50% young (3 Gyr) objects. The age distribution is compared to the complete set of simulations, as used for comparison to the observed globular cluster systems. The number of objects in both age populations is given on top of each panel. The different models were picked randomly out of a set of 1000 simulations.

second generation globular clusters is derived with 1–1.5 Gyr. The size ratio between both age populations is similar to that in NGC 4365.

5. Discussion and summary

In this study we extend previously obtained optical and near-infrared observations towards the shorter wavelength range (U-band) in order to increase the age resolution in color–color distributions. This goal has been achieved, the distribution of the globular clusters in $(U - I)$ vs. $(V - K_s)$ color plots allows a much better age determination than in $(V - I)$ vs. $(V - K_s)$ plot. If we apply a semi-numerical approach to derive the age structure in globular cluster systems the higher age resolution for the remaining globular cluster samples is confirmed.

In Sect. 3.3 we discussed the various new bias effects introduced by the U-band in the method. These hamper a correct interpretation of the derived size ratios between the cluster sub-populations. The spatial bias can be reduced by spatial extended surveys, which include as well globular clusters at larger galactocentric distances. The selection effect introduced by the limiting magnitudes in the U and K bands could be removed by even deeper observations but this is currently the limiting aspect of the method. We summerise that the derived size of the young/intermediate age globular cluster population in both galaxies has to be considered as an upper limit, even more so, since the diffuse galaxy light does not show evidence for a dominant 1–5 Gyr old stellar population. Nevertheless, our conclusion of a second star formation event during the galaxies evolutions is supported by morphological features. In NGC 4365 a counter-rotating core has been detected (e.g. Wagner et al. 1988; Bender et al. 1994; Davies et al. 2001), wheras in the center of NGC 5846 prominent dust filaments have been found (Goudfrooij & Trichnieri 1998). Our original intension to use the size of the sub-populations to draw conclusions on the formation scenario for a given early-type galaxy would require very deep, wide-field data, e.g. as can be hoped for by the advent HAWK-I on the VLT which will provide an near-infrared counter-part to the typical field-of-view of optical instruments on 8 to 10 m-class telescopes.

For now, the addition of the U-band "only" improves the age resolution by a significant amount. From this, we determine very young average ages for the young metal-rich globular cluster sub-populations in NGC 4365 and NGC 5846 of ∼2 and 1−1.5 Gyr, respectively. Both early-type galaxies must have experienced a significant star formation episode very recently, forcing us to re-think the global star formation histories of at least some early-type galaxies. How representative these two galaxies are will be discussed in a sub-sequent paper discussing a larger sample of galaxies.

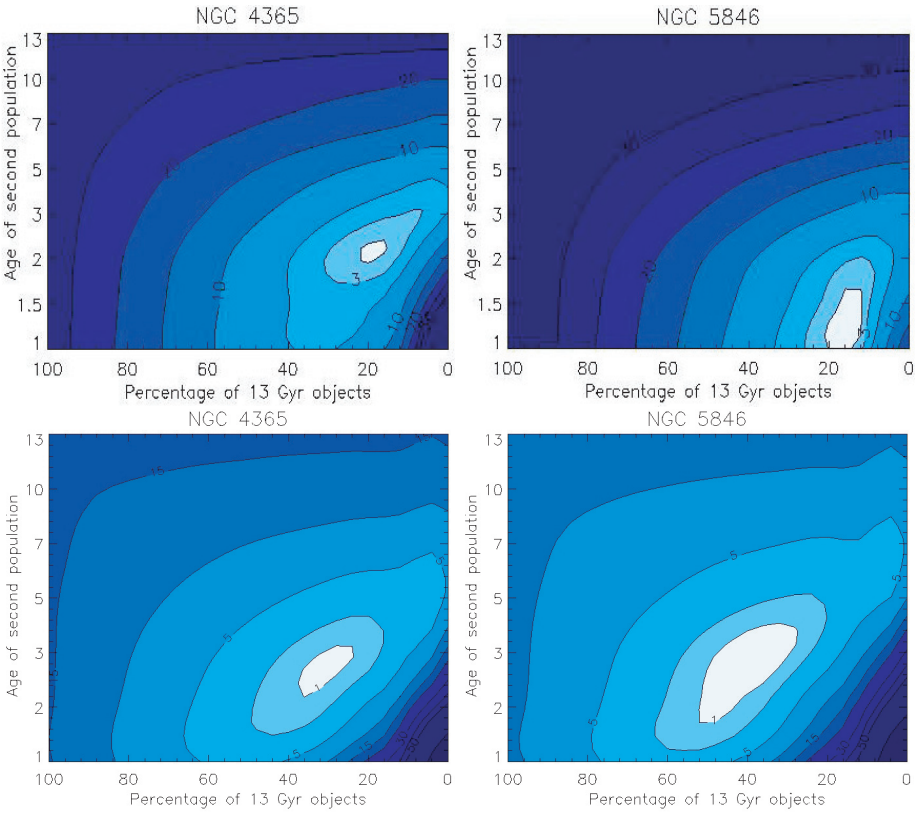

Fig. 11. Results of the comparison between the observed globular cluster systems of NGC 4365 (*left*) and NGC 5846 (*right*) and simulated systems. The top panel represent the χ^2 test results using age distributions derived from $(U-I)$ vs. $(V-K_s)$ color–color diagrams compared to the $(V-I)$ vs. $(V-K_s)$ results shown in the lower panels.

References

Anders, P., Bissantz, N., Fritze-v.Alvensleben, U., et al. 2004, MNRAS, 347, 196

Ashman, K. M., & Zepf, S. E. 1992, ApJ, 384, 50

Ashman, K. M., Bird, C. M., & Zepf, S. E. 1994, AJ, 108, 2348

Bender, R., Saglia, R. P., & Gerhard, O. E. 1994, MNRAS, 269, 785

Bennett, C. L., Halpern, M., Hinshaw, G., et al. 2003, ApJS, 148, 1

Bertin, E., & Arnouts, S. 1996, A&AS, 117, 393

Bruzual, A. G., & Charlot, S. 1993, AJ, 405, 538

Bruzual, A. G., & Charlot, S. 2000, private communications

Bruzual, A. G., & Charlot, S. 2003, MNRAS, 344, 1000

Buta, R., & Williams, K. L. 1995, AJ, 109, 543

Davies, R. L., Kuntschner, H., Emsellem, E., et al. 2001, ApJ, 548, L36

de Vaucouleurs, G., de Vaucouleurs, A., Corwin, H. G., et al. 1991, Third Ref. Catalogue of Bright Galaxies (New York: Springer)

Frogel, J. A., Persson, S. E., Matthews, K., et al. 1978, ApJ, 220, 75

Goudfrooij, P., & Trinchieri, G. 1998, A&A, 330, 123

Hempel, M., Hilker, M., Kissler-Patig, M., et al. 2003, A&A, 405, 487, Paper III

Hempel, M., & Kissler-Patig, M. 2004, A&A, 419, 863, Paper IV

Hibbard, J. E., & Mihos, J. C. 1995, AJ, 110, 140

Kissler-Patig, M., Brodie, P. B., & Minniti, D. 2002, A&A, 391, 441 (Paper I)

Maraston, C. 2000, priv. communication

Puzia, T. H., Zepf, S. E., Kissler-Patig, et al. 2002, A&A, 391, 453 (Paper II)

Schlegel, D. A., Finkbeiner, D. P., & Davis, M. 1998, ApJ, 500, 525

Schweizer, F., & Seitzer, P. 1998, AJ, 116, 2206

Spergel, D. N., Verde, L., Peiris, H. V., et al. 2003, ApJS, 148, 175

Tonry, J. L., Dressler, A., Blakeslee, J. P., et al. 2001, ApJ, 546, 681

Vazdekis, A. 1999, ApJ, 513, 224

Wagner, S. J., Bender, R., & Möllenhoff, C. 1988, A&A, 195, L5

Worthey, G. 1994, ApJS, 95, 107